

Supervised Auto-Encoding Twin-Bottleneck Hashing

Yuan Chen*¹ and Stéphane Marchand-Maillet¹

¹University of Geneva, Geneva, Switzerland
ychen169@ucr.edu

Abstract

Deep hashing has shown to be a complexity-efficient solution for the Approximate Nearest Neighbor search problem in high dimensional space. Many methods usually build the loss function from pairwise or triplet data points to capture the local similarity structure. Other existing methods construct the similarity graph and consider all points simultaneously. Auto-encoding Twin-bottleneck Hashing is one such method that dynamically builds the graph. Specifically, each input data is encoded into a binary code and a continuous variable, or the so-called twin bottlenecks. The similarity graph is then computed from these binary codes, which get updated consistently during the training. In this work, we generalize the original model into a supervised deep hashing network by incorporating the label information. In addition, we examine the differences of codes structure between these two networks and consider the class imbalance problem especially in multi-labeled datasets. Experiments on three datasets yield statistically significant improvement against the original model. Results are also comparable and competitive to other supervised methods.

1. Introduction

In the age of information explosion, storing massive data and retrieving relevant samples from the dataset in high dimensional space are fundamental topics in both the academic and industrial communities. Learning to hash is one promising solution and has gained lots of attention. The hashing method aims to map complex input data into compact binary codes, which respect the local similarity structure of the original space. This way, time-consuming distance computation in the Euclidean space can be approximately replaced by the simple hamming distance computation in the binary space, which can be performed efficiently in the hardware using the CPU instruction [35]. In addition,

storing binary codes instead of original data also reduces the burden on the storage requirement.

Existing hashing methods can be roughly divided into traditional methods and deep hashing. Traditional methods [38][23][34][11][14][41] take feature vectors as input and engineer a hash function with parameters, which can be optimized by a loss function. In contrast, deep hashing [22][8][20][19][26] takes advantage of neural networks to extract features and plays the role of hash function thanks to its powerful ability of simulating complicated functions. The network parameters are optimized by the loss function, and this strategy has demonstrated superior performance over the traditional methods. Deep methods can also again fall into unsupervised methods [22][26][42] and supervised methods [8][19][36][20][25][40][2][37].

Since the hash function needs to preserve the neighborhood structure of the input space, existing methods usually involve similarity terms computed from the pair or triplet of data points, or construct the similarity graph. Jie Qin et al. [26] pointed out that these methods could suffer from the "static graph" problem where the pre-computed graph would bring biased prior knowledge and could not be updated to capture the intrinsic data structure, leading to sub-optimal performance. To address the problem, Twin-Bottleneck Hashing (TBH) [26] introduces twin bottlenecks: the binary bottleneck (BinBN) and the continuous bottleneck (ConBN). The similarity graph is constructed directly from the binary codes and gets updated during the training process to better model the data structure. In addition, the ConBN could help improve the reconstruction quality in the decoder, and the reconstruction loss of the decoder is optimized as a score to quantify the encoder quality. However, minimizing the reconstruction loss only provides an implicit guide/direction on optimizing the binary codes, and the back-propagation pathway flows from the decoder to the GCN network [15] before reaching the encoder. In other words, the binary codes may not receive adequate guidance to be updated. On the other hand, class labels are not considered in the model, and the architecture

*Corresponding Author

is too weak to operate self-supervision. In fact, label information is important for the hashing problem, since it acts as an independent description for data points besides the information captured by the feature vectors, which complements to provide a more complete view of the same object and help encode binary codes of better quality.

As a solution to the above problems, this paper proposes the Supervised Twin-Bottleneck Hashing (STBH). Based on the original TBH model, we introduce a classification layer built on top of the binary bottleneck to incorporate the semantic information. This brings a number of benefits. First, the binary codes receive direct optimizing direction from the classification loss term. Second, supervised information mitigates the semantic gap and makes the distinction of codes better separated between different classes. Third, the loss function also introduces robustness when the extracted features incorrectly reflect the distance relation with respect to its neighbors. The main contributions of this work are summarized as follows:

- A classification layer is proposed on top of the binary bottleneck of the TBH model to include the label information.
- We study and compare the codes structures between the two networks to show the benefits brought by the supervised learning.
- We consider the class imbalance problem in multi-label datasets, which are hardly mentioned previously.
- Experiments conducted on three datasets show superior performances compared to the original model.

2. Related Work

The proposed STBH is mostly related to the TBH model [26], and thus inherits the same competing techniques.

TBH model [26] is one of unsupervised deep hashing with encoder-decoder architecture. A twin-bottleneck is incorporated to construct an adaptive similarity graph and mitigate the reconstruction loss of the decoder component. In addition, a stochastic neuron [27] is utilized to allow the standard back-propagation process while preserving the binary constraints. In order to achieve the balanced and independent binary codes, the model involves Wasserstein Auto-Encoders (WAE) [32] to regulate the binary variables adversarially. As discussed above, the binary codes are implicitly optimized by the reconstruction loss, and the absence of the semantic information could also lead to sub-optimal performance.

3. Proposed Method

3.1. Notations and TBH

Our STBH is established based on the unsupervised TBH model [26]. We first introduce notations as well as the TBH network briefly.

The network structure is illustrated in Fig. 1. First, feature vectors, denoted by $\mathbf{x} \in \mathbb{R}^D$, are extracted from the input raw data. Then the feature vector is fed to the encoder to generate two latent variables: a M -bit binary code \mathbf{b} , and a L dimensional continuous variable \mathbf{z} . Specifically:

$$\begin{aligned} \mathbf{b} &= \alpha(f_1(\mathbf{x}; \theta_1), \epsilon) \in \{0, 1\}^M, \\ \mathbf{z} &= f_2(\mathbf{x}; \theta_2) \in \mathbb{R}^L \end{aligned} \quad (1)$$

where f_1 and f_2 indicate the two encoding functions, and θ_1 and θ_2 are the corresponding layer parameters of f_1 and f_2 . In addition, to implement the standard back-propagation (BP) process with binary constraints, the discrete stochastic neuron activation $\alpha(\cdot, \epsilon)$ [27] is utilized to produce binary codes and defined as:

$$b^i = \alpha(f_1(\mathbf{x}; \theta_1), \epsilon)^i = \begin{cases} 1 & f_1(\mathbf{x}; \theta_1)^i \geq \epsilon^i, \\ 0 & f_1(\mathbf{x}; \theta_1)^i < \epsilon^i \end{cases} \quad (2)$$

where the superscript i indicate the i -th component of the vector, and variables ϵ conform to the uniform distribution $\mathcal{U}(0, 1)^M$.

For simplicity, we consider a batch of N_B data points, and denote corresponding continuous variables \mathbf{Z}_B and binary codes \mathbf{B}_B as:

$$\begin{aligned} \mathbf{Z}_B &= [\mathbf{z}_1; \mathbf{z}_2; \dots; \mathbf{z}_{N_B}] \in \mathbb{R}^{N_B \times L} \\ \mathbf{B}_B &= [\mathbf{b}_1; \mathbf{b}_2; \dots; \mathbf{b}_{N_B}] \in \{0, 1\}^{N_B \times M} \end{aligned} \quad (3)$$

Subsequently, the similarity graph \mathbf{A} can be computed from binary codes of the training batch by:

$$\begin{aligned} \mathbf{A} &= \mathbb{J} + \frac{1}{M} (\mathbf{B}_B (\mathbf{B}_B - \mathbb{J})^T + (\mathbf{B}_B - \mathbb{J}) \mathbf{B}_B^T) \\ &\in [0, 1]^{N_B \times N_B} \end{aligned} \quad (4)$$

where \mathbb{J} is a $N_B \times N_B$ matrix with all elements equal to 1. Later, the graph and the continuous variables are processed by the GCN network [15] to generate the latent variables \mathbf{Z}'_B for reconstruction:

$$\begin{aligned} \mathbf{Z}'_B &= \text{sigmoid} \left(\mathbf{D}^{-\frac{1}{2}} \mathbf{A} \mathbf{D}^{-\frac{1}{2}} \mathbf{Z}_B \mathbf{W}_{\theta_3} \right) \\ &\in (0, 1)^{N_B \times L} \end{aligned} \quad (5)$$

where \mathbf{W}_{θ_3} is a $L \times L$ matrix of parameters of the GCN network. In addition,

$$\mathbf{D} = \text{diag}(\mathbf{A} \mathbf{1}^T) \quad (6)$$

where $\mathbf{1}$ is a N_B -dimensional vector full of 1s. Finally \mathbf{Z}'_B is fed into the decoder for the reconstruction of feature vectors:

$$\hat{\mathbf{x}} = g(\mathbf{z}'; \theta_4) \in \mathbb{R}^D \quad (7)$$

where $g(\cdot; \theta_4)$ indicates the decoding function and θ_4 is the

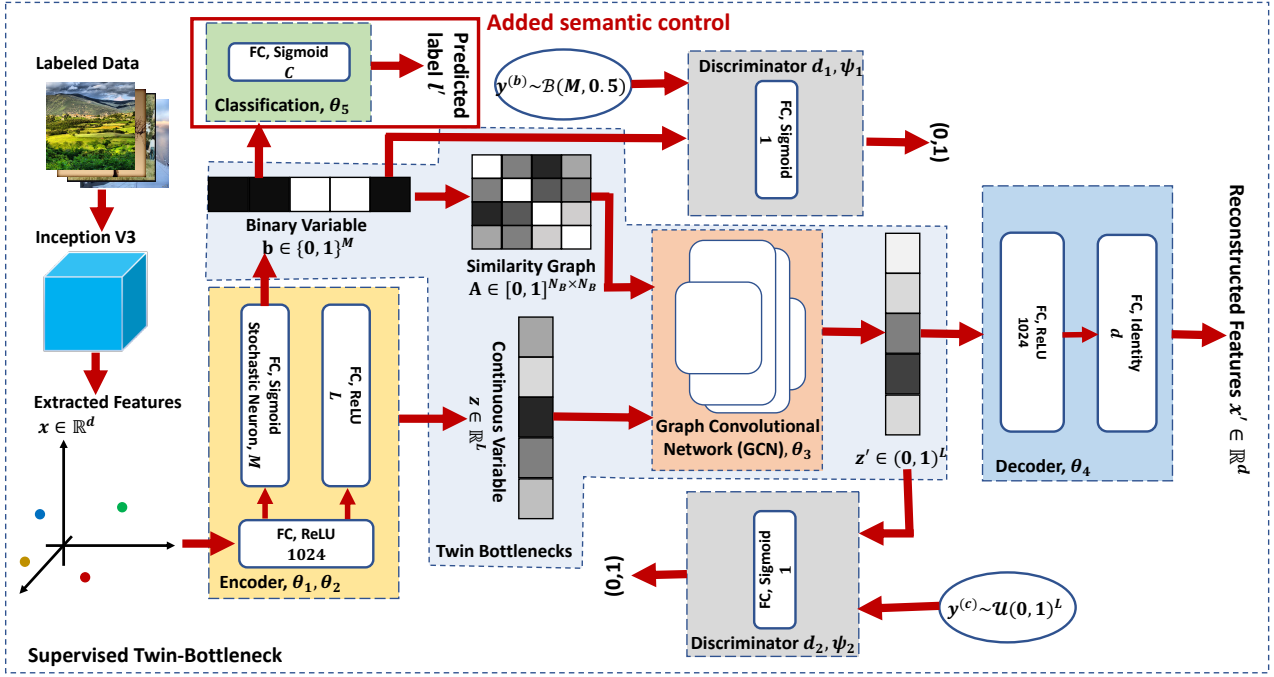


Figure 1. The schematic of STBH. A classification layer is directly added on top of the binary bottleneck to instill the semantic information. The number of classes is denoted as C . Other modules follow the pattern of the original TBH model.

corresponding parameters.

In addition, to encourage latent variables to fully explore the latent spaces, two WAEs [32] are utilized to adversarially regulate variables with two discriminators: $d_1(\cdot; \psi_1)$ and $d_2(\cdot; \psi_2)$ where ψ_1 and ψ_2 are corresponding parameters. Specifically, $d_1(\cdot; \psi_1)$ is used for the binary codes \mathbf{b} to achieve the bit balance and independence, while $d_2(\cdot; \psi_2)$ is employed for the latent variables \mathbf{z}' :

$$\begin{aligned} d_1(\mathbf{b}; \psi_1) &\in (0, 1); & d_1(\mathbf{y}^b; \psi_1) &\in (0, 1) \\ d_2(\mathbf{z}'; \psi_2) &\in (0, 1); & d_2(\mathbf{y}^c; \psi_2) &\in (0, 1) \end{aligned} \quad (8)$$

where \mathbf{y}^b conforms to binomial distribution $\mathcal{B}(M, 0.5)$ and \mathbf{y}^c is sampled from the uniform distribution $\mathcal{U}(0, 1)^L$.

3.2. Supervised TBH

As shown in Fig. 1, we propose to add a classification layer directly on top of the binary variables, which consists of one fully connected layer with sigmoid as its activation function. The predicted label l^c can be expressed as:

$$l^c = \text{sigmoid}(\mathbf{W}_{\theta_5} \mathbf{b}) \in [0, 1]^C \quad (9)$$

where $\mathbf{W}_{\theta_5} \in \mathbb{R}^{C \times M}$ indicates the projection matrix and C is the number of classes. This classifier can not only introduce the direct guidance on the binary codes, but also provide semantic information to make codes distribution of different classes more distinguishable, which could help improve the codes quality. We detail how this semantic control

is incorporated into the loss function in the next section.

3.3. Loss Function

3.3.1 Discriminating Objective

The Discriminating objective \mathcal{L}_D is defined by:

$$\begin{aligned} \mathcal{L}_D = & \frac{1}{N_B} \sum_{i=1}^{N_B} (\log d_1(\mathbf{y}_i^b; \psi_1) \\ & + \log(1 - d_1(\mathbf{b}_i; \psi_1)) \\ & + \log d_2(\mathbf{y}_i^c; \psi_2) + \log(1 - d_2(\mathbf{z}'_i; \psi_2))) \end{aligned} \quad (10)$$

\mathcal{L}_D is optimized to train two discriminators over the parameter space $\{\psi_1, \psi_2\}$ such that they could distinguish the distributions of codes generated by the encoder from those sampled from the targeted distributions.

3.3.2 Auto-Encoding Objective

The Auto-Encoding objective \mathcal{L}_{AE} is defined as:

$$\begin{aligned} \mathcal{L}_{AE} = & \frac{1}{N_B} \sum_{i=1}^{N_B} \mathbb{E}_{\mathbf{b}_i} \left[\frac{1}{D} \|\mathbf{x}_i - \mathbf{x}'_i\|^2 \right. \\ & + \lambda \log d_1(\mathbf{b}_i) + \lambda \log d_2(\mathbf{z}'_i) \\ & \left. + \gamma \|\mathbf{1}_i - \mathbf{l}'_i\|^2 \right] \\ & + \eta \|\mathbf{W}_{\theta_5}\|_{1,1} \end{aligned} \quad (11)$$

where \mathbf{l} denotes the true label, λ , γ and η are hyper-parameters to control the weights of the discriminating loss, the regression loss and the regularization of classifier’s weights respectively. $\mathbb{E}_{\mathbf{b}_i}$ means the expectation over the latent binary code \mathbf{b} since \mathbf{b} is generated from a sampling process. Specifically, the first line of \mathcal{L}_{AE} is the reconstruction loss, which scores the encoder quality and optimizes binary codes to preserve the local structure of the input feature space. The second line is the discriminating loss to encourage distributions of generated variables \mathbf{b} and \mathbf{z}' resemble more the targeted distributions to maximize the entropy. The third line is the regression loss, which provides the direct semantic information to separate codes structure more for different labels. The fourth line is the regularization term of the classifier’s weights to simplify the network parameters and avoid overfitting. Overall, \mathcal{L}_{AE} is optimized over the parameter space $\{\theta_1, \theta_2, \theta_3, \theta_4, \theta_5\}$ to train the binary codes of good quality.

3.4. Out-of-Sample Extension

After STBH is trained, given an unknown data \mathbf{x}^q , its binary codes \mathbf{b}^q can be generated by the encoder of the network as follows:

$$\mathbf{b}^q = (\text{sgn}[f_1(\mathbf{x}^q; \theta_1) - 0.5] + 1) / 2 \in \{0, 1\}^M \quad (12)$$

In fact, it is a special case of Eqn. 2 where the random variable ϵ^i is fixed to 0.5.

4. Experiments

We evaluate the performance of STBH model on three widely used image benchmarks: CIFAR-10, NUS-WIDE and MS-COCO such that we can make comparisons with the original TBH and other papers.

4.1. Implementation Details

The model is implemented with Tensorflow [1], and the code for the TBH network is forked from the original TBH paper [26]. A convolutional network called InceptionV3 [28] is utilized here to extract the features from all datasets. For the experimental parameters, we set the training batch size to 1500, and the length of binary codes $M = 32$. In addition, we do a grid search to fine-tune the weights γ and η . Other parameters follow the TBH paper [26]. Besides, we perform a six-fold cross validation for all experiments and report the average for the fair comparisons. Our implementation code can be found at <https://github.com/Wallace-Chen/TBH/tree/supervised>.

4.2. Datasets

CIFAR-10 [17] is a single-label dataset with 60,000 images from 10 classes. We randomly sample 10,000 images as the query set and the remaining 50,000 images as the

training set. The dataset analysed during the current study is available at <https://www.cs.toronto.edu/kriz/cifar.html>.

NUS-WIDE [7] is a multi-label dataset consisting of 269,648 images from 81 labels. Following the setting in the paper [39], we select a subset of images from 21 most frequent labels, where the number of images associated with the tag is at least 5,000. From the subset, we randomly choose 10,000 images as the query set and 50,000 images as the training set. The dataset analysed during the current study is available at <https://lms.comp.nus.edu.sg/wp-content/uploads/2019/research/nuswide/NUS-WIDE.html>.

MS-COCO [21] is another multi-label dataset. Here, we adopt the 2014 train/val set with 12,2218 images of 80 categories. However, we observe that the "person" label dominates among all classes. For example, as shown in Fig. 2, more than half of the images are associated with the "person" label. This would be a serious class-imbalance issue when we apply the supervised learning (for more discussions see 4.5). Since the dataset is multi-labeled, it is not trivial to rebalance different classes. We decided to remove the "person" class and also the images labeled with this class. We randomly pick 8,000 images as the query set and another 40,000 images as the training set from the remaining set. The resulting label distribution is shown in Fig. 4(c). The dataset analysed during the current study is available at <https://cocodataset.org/#download>.

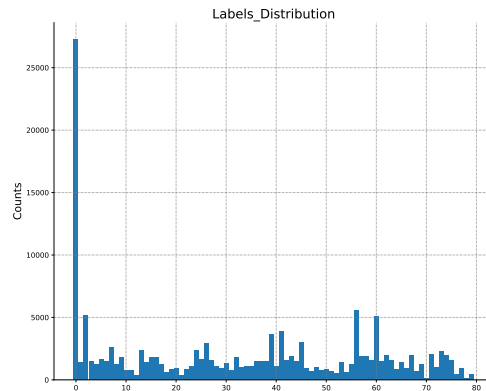


Figure 2. Label distribution of randomly chosen 50,000 images from MS-COCO dataset with 80 classes. More than half of images are associated by the 'person' (first) label.

4.3. Metrics

To evaluate the performance of our model, we adopt the standard metrics: Precision w.r.t. top 1000 returned items (P@1000), Precision-Recall curve, and mean Average Precision (mAP). For multi-label datasets (NUS-WIDE and MS-COCO), we regard two items similar when they share at least one common label. In addition, we report the av-

erage and the standard deviation to have a fair comparison between the STBH and TBH models. To make the comparison statistically significant, p-value (see Appendix A for the details) is computed for the STBH against the TBH model.

4.4. Results Comparison

To compare our STBH model to the original TBH model, we keep every condition the same except turning on the regression and regularization term in the loss function for STBH. In addition, a grid search on the value of $\gamma = \eta$ is performed for each dataset.

The results of P@1000 and mAP are reported in Table 1 and 2 respectively, while the P-R curves are shown in Fig. 3. The performance of our proposed STBH gets much improved compared to the original TBH model when γ and η are carefully chosen. For example, setting $\gamma = \eta = 20$ for the CIFAR-10 and NUS-WIDE, and $\gamma = \eta = 30$ for the MS-COCO are good options to achieve a remarkable improvement. From the point of view of p-value, if we set the significance level to 0.05, the above numbers can also give us p-values below or around the significance level, which means results of STBH are better than those of TBH at the confidence level of 95%. The great improvements demonstrate the view that semantic supervision is very helpful and powerful for solving the hashing problem and can provide extra information other than that contained in the features extracted from the raw dataset.

4.5. Class Imbalance

Another observation from the above results is that the performance improvement of the CIFAR-10 dataset is the greatest among the three datasets because we have a more balanced class distribution in CIFAR-10, as shown in Fig. 4. The class imbalance in the other two multi-label datasets NUS-WIDE and MS-COCO affects the ability of supervised learning.

The uneven class distribution has been a challenge for the classification problem, as the design of most classifiers aims to reduce the global error, which tends to benefit and gets biased towards the majority class, leading to the poor accuracy on the minority examples and underperformance [16][9][3]. There exist many works that try to solve the problem in the multi-label datasets, which can be categorized into three approaches [3]: algorithmic adaptations, ensemble-based methods and resampling techniques. Algorithmic adaptations [12][18][31][6] aim to design classifiers insensitive to the imbalanced datasets and are mostly specific to the domains considered in the problem. Ensemble-based methods [29][30] normally build ensembles of classifiers and then obtain a final prediction. However they require the training of many classifiers and suffer from low efficiency. Resampling techniques [13][4][10] instead focus on preprocessing of the dataset to produce a more balanced

version, and involve undersampling or/and oversampling. MLSTMOTE [3], for example, is one of extensions of original SMOTE [5] method designed for multi-label datasets.

For the datasets used in this paper, NUS-WIDE and MS-COCO are multi-label datasets and have skewed class distributions. Especially the imbalance ratio of MS-COCO is quite extreme (1:1000 for some classes) even after the dominated label "person" is removed. A more careful treatment of such imbalance problems is needed for a better performance and left for further work.

4.6. Complexity

The benefit brought by incorporating label information is remarkable, while the change in the network architecture is minimal, as indicated in Fig. 1. In this section, we show in fact the overhead of running the STBH model is also negligible or small compared to the TBH model in terms of training time, total loss and the memory used.

In Fig. 5, the upper plots show the running time over the training steps between TBH and STBH on three datasets, which demonstrates that the STBH model takes the almost same time as the TBH model independent of datasets. The computing platform used is equipped with a 3.6GHz Intel i3-8100 CPU, 32 GB RAM, and NVIDIA RTX 2070.

The lower plots in Fig. 5 give the evolution of total training loss between TBH and STBH. As can be clearly seen, the losses are converged at the end of the training, especially compared to those at the start. In addition, STBH can be optimized within the same training steps and does not need extra epochs. Moreover, a closer observation on the subfigure 5(d) reveals that STBH with small values of $\gamma(\eta)$ (less than 30 for example) can actually achieve even lower losses than the TBH model. This validates the view that supervision of class labels can provide complementary information and help guide the optimization to find a better solution in the search space.

We also point out here that STBH requires little extra memory space during the training, which can be illustrated by the number of network parameters to be trained. The original TBH model contains 5,543,490 parameters regardless of datasets, while STBH only needs a few hundreds (CIFAR-10, NUS-WIDE) or thousands (MS-COCO) more parameters, which are negligible. The exact numbers can be found in Table 3.

It is worthwhile to emphasize that STBH can achieve considerable improvements at virtually little extra cost.

4.7. Grid Search on η

We keep $\eta = \gamma$ during the above grid searches, however we could also fine tune the value of η while fixing the γ . Since η is the weight of the regularization term of the classifier's weights, we aim to find a proper number of η such that the regularization term could get decreased to avoid the

Table 1. Performance comparison in terms of P@1000 Between the TBH model and STBH model with various $\gamma = \eta$

Method	CIFAR-10			NUS-WIDE			MS-COCO ("person" label removed)		
	mean	s.t.d.	p-value	mean	s.t.d.	p-value	mean	s.t.d.	p-value
TBH	0.590	0.010	-	0.680	0.004	-	0.670	0.008	-
STBH, $\gamma = \eta = 1$	0.600	0.010	0.4452	0.706	0.005	0.2772	0.680	0.008	0.434
STBH, $\gamma = \eta = 10$	0.710	0.008	0.0468	0.789	0.002	0.0050	0.703	0.011	0.308
STBH, $\gamma = \eta = 20$	0.796	0.004	0.0031	0.808	0.004	0.0031	0.727	0.028	0.266
STBH, $\gamma = \eta = 30$	0.832	0.005	0.0012	0.826	0.004	0.0013	0.769	0.009	0.064
STBH, $\gamma = \eta = 40$	0.852	0.002	0.0008	0.838	0.004	0.0008	0.765	0.013	0.092
STBH, $\gamma = \eta = 50$	0.861	0.003	0.0006	0.845	0.003	0.0003	0.764	0.009	0.077

Table 2. Performance comparison in terms of mAP Between the TBH model and STBH model with various $\gamma = \eta$

Method	CIFAR-10			NUS-WIDE			MS-COCO ("person" label removed)		
	mean	s.t.d.	p-value	mean	s.t.d.	p-value	mean	s.t.d.	p-value
TBH	0.636	0.009	-	0.703	0.004	-	0.570	0.010	-
STBH, $\gamma = \eta = 1$	0.650	0.008	0.4216	0.733	0.005	0.2447	0.580	0.009	0.447
STBH, $\gamma = \eta = 10$	0.750	0.007	0.0440	0.811	0.002	0.0052	0.630	0.012	0.222
STBH, $\gamma = \eta = 20$	0.824	0.003	0.0034	0.827	0.003	0.0014	0.653	0.025	0.198
STBH, $\gamma = \eta = 30$	0.851	0.005	0.0017	0.842	0.003	0.0014	0.696	0.006	0.038
STBH, $\gamma = \eta = 40$	0.865	0.002	0.0011	0.853	0.004	0.0011	0.695	0.014	0.064
STBH, $\gamma = \eta = 50$	0.873	0.003	0.0009	0.859	0.002	0.0005	0.695	0.009	0.049

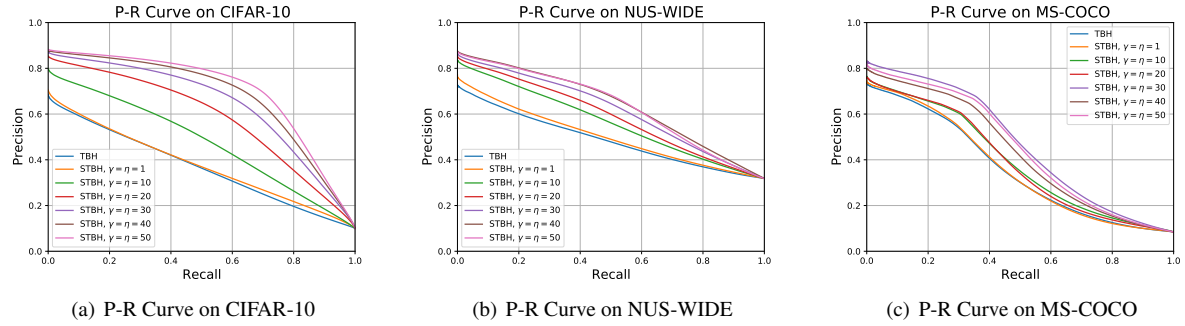


Figure 3. Comparisons of P-R Curves for the CIFAR-10 (left), NUS-WIDE (middle), and MS-COCO (right)

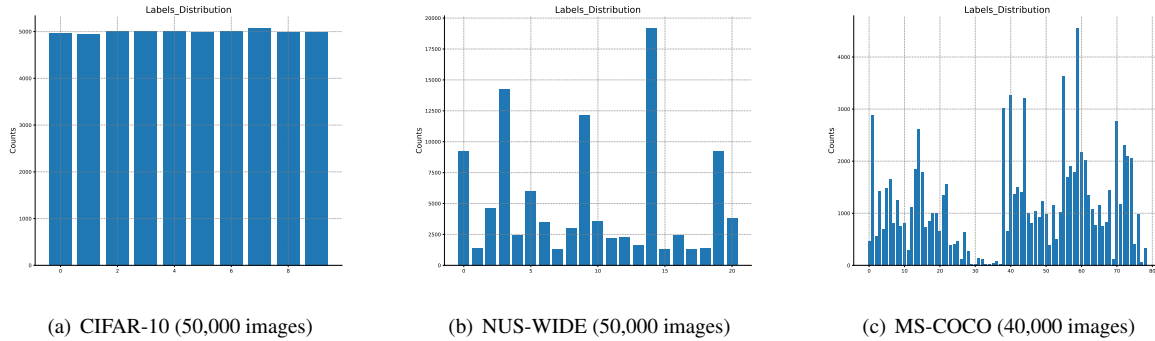
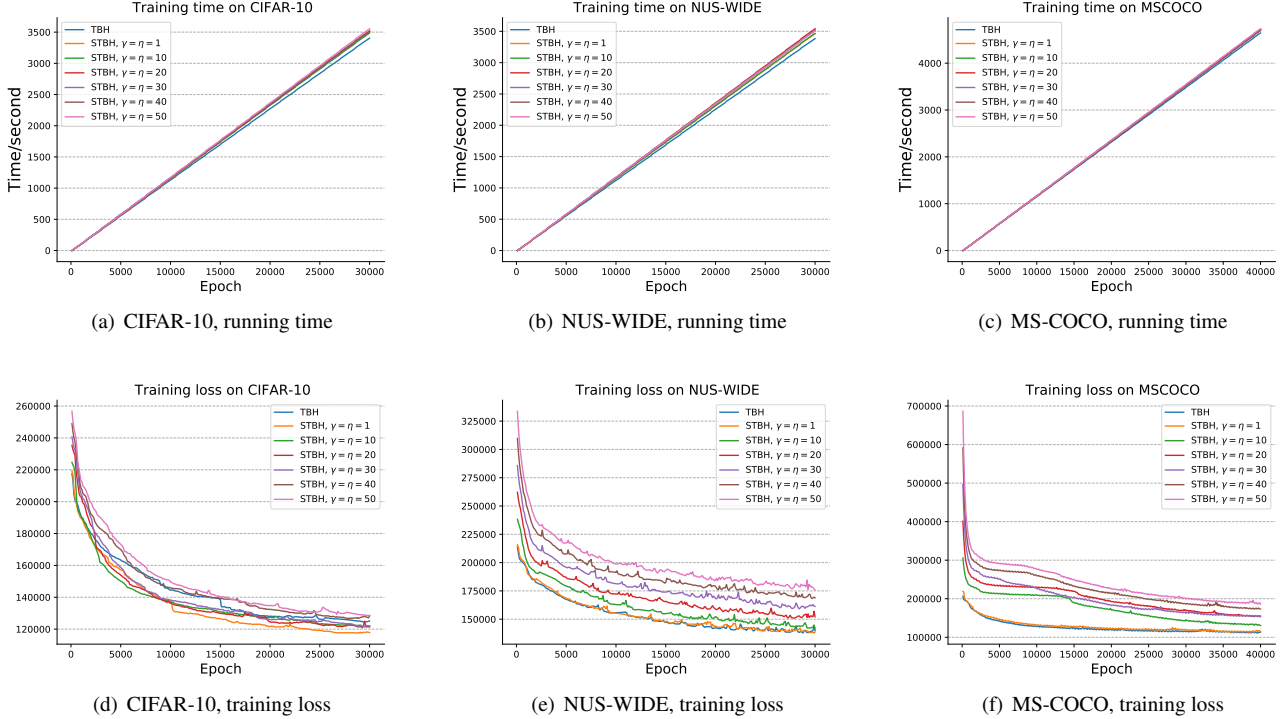


Figure 4. Class distributions for the CIFAR-10 (left), NUS-WIDE (middle), and MS-COCO (right). X-axis indicates the class ID while the Y-axis is the counts. CIFAR-10 has the most balanced class distribution.

Table 3. Number of network parameters to be trained.

	TBH	STBH + CIFAR-10	STBH + NUS-WIDE	STBH + MS-COCO
Number of parameters	5,543,490	5,543,820	5,544,183	5,546,097

Figure 5. Comparisons of training times (upper) and losses (lower) between TBH and STBH with various values of $\gamma(\eta)$ on three datasets.

overfitting. As shown in Fig. 6, for the CIFAR-10 dataset, the subplots 6(a) and 6(b) are regularization terms for different η values with $\gamma = 20$. We can decrease the regularization term by varying the values of η , and the subplots 6(c) and 6(d) are the heat maps showing the classifier’s weights \mathbf{W}_{θ_5} for the corresponding η values respectively. By setting $\eta = 100$ instead of 20, the L1 norm of \mathbf{W}_{θ_5} get much decreased and the parameters are simplified. The price is that the performance of $\eta = 100$ gets lowered a bit, but still close to that of $\eta = 20$, as can be observed in Table 4.

4.8. Correlation Matrix of Labels

We have seen above that the Supervised TBH performs better than the original TBH model in terms of P@1000, P-R curve and mAP. As also mentioned, supervised learning could also help separate the codes’ distributions for different labels since class labels can provide more accurate classification information. In other words, the correlation between different classes in STBH is expected to be lower than that of TBH. We show such plots of correlation matrices in Fig. 7, where we can see that the STBH (lower) generally has lower correlations. Note that for the STBH

model, we choose the proper values of η and γ by grid searches for each of the three datasets. In Fig. 8, we take the absolute value of correlations, and plot the histograms of these numbers. Compared to the TBH model (upper), STBH (lower) mitigates strong correlations and shift the peak to the left. To quantify such differences, in Table 5, we report the median, mean and standard deviation of these histograms between TBH and STBH models. From the table, we can again observe that the STBH helps untangle correlations and better discriminate between different labels.

4.9. Visualization

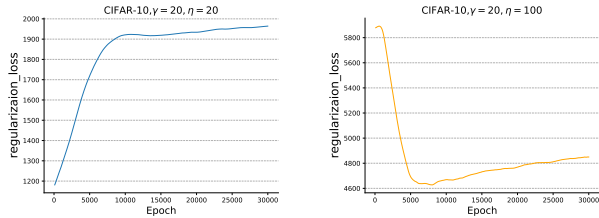
To give an intuition on the discriminating power of the STBH model, Fig. 9 shows the t-SNE (upper) [33] and UMAP (lower) [24] visualization results on CIFAR-10 between TBH (left) and STBH (right) model. t-SNE is a popular technique to visualize high-dimensional data. UMAP is a novel algorithm for dimension reduction and visualization, but unlike t-SNE that pays more attention to the preservation of local distances, UMAP preserves more of the global structure of datasets [24]. In Fig. 9, we can clearly observe that STBH can better group data points of

Table 4. Performance comparison on CIFAR-10 with different η values.

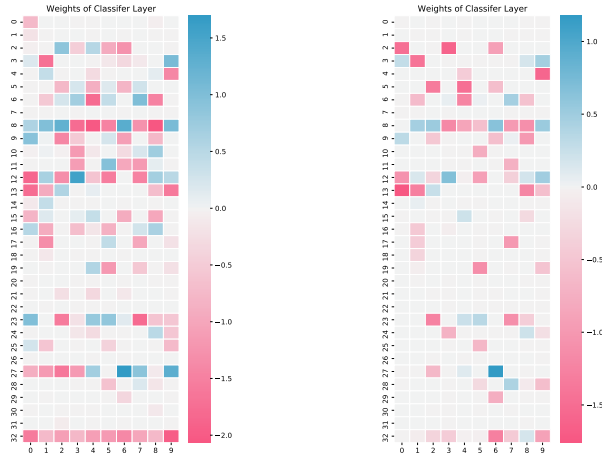
Method	P@1000			mAP		
	mean	std.	p-value	mean	std.	p-value
TBH	0.590	0.010	-	0.636	0.009	-
STBH, $\gamma = 20, \eta = 20$	0.824	0.002	0.0034	0.796	0.004	0.0031
STBH, $\gamma = 20, \eta = 100$	0.802	0.002	0.0065	0.773	0.003	0.0055

Table 5. Median, mean and standard deviation of absolute values of the correlations for the TBH model and STBH model with the chosen η, γ values.

	CIFAR-10		NUS-WIDE		MS-COCO	
	TBH	STBH, $\eta = 100, \gamma = 20$	TBH	STBH, $\eta = 20, \gamma = 10$	TBH	STBH, $\eta = 30, \gamma = 30$
Median	0.349	0.203	0.461	0.347	0.353	0.275
Mean	0.301	0.232	0.501	0.388	0.395	0.319
Std	0.213	0.171	0.280	0.250	0.255	0.235



(a) Regularization term: $\gamma = \eta = 20$ (b) Regularization term: $\gamma = 20, \eta = 100$



(c) Classifier’s weights: $\gamma = \eta = 20$ (d) Classifier’s weights: $\gamma = 20, \eta = 100$

Figure 6. Regularization term (upper) and the classifier’s weights (lower) for $\eta = 20$ (left) and $\eta = 100$ (right) while fixing $\gamma = 20$, CIFAR-10 dataset.

the same label together while pushing away samples from different labels with very clear boundaries. This illustrates

the powerful discriminating ability of STBH due to the incorporated label information.

4.10. Comparison with Existing Supervised Methods

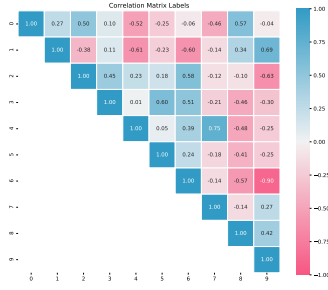
In the end, we also compare our STBH model with other existing state-of-art supervised deep hashing methods. For a fair comparison, we report results of binary codes with 32 bits for all methods, and numbers are adopted from their papers. Since we remove the "person" label from the MS-COCO dataset, MS-COCO is not included in the comparison. The mAP results are shown in Table 6, and the compared deep methods include: DTSH [36], DPSH [20], DSDH [19], DRLIH [25], PGDH [40], HBMP [2] and DRL-LER [37]. From Table 6, our results are comparable to the state-of-art performances, especially STBH outperforms all other methods on the NUS-WIDE dataset.

Table 6. Performance comparisons of mAP with other Supervised Deep Hashing.

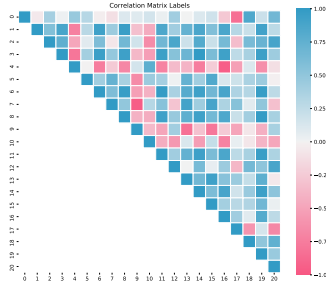
Methods	CIFAR-10	NUS-WIDE
DTSH	0.925	0.785
DPSH	0.795	0.736
DSDH	0.939	0.820
DRLIH	0.855	0.845
PGDH	0.741	0.780
HBMP	0.830	0.822
DRL-LER	0.952	0.837
Ours (STBH, $\eta = \gamma = 50$)	0.873	0.859

5. Conclusion

In this paper, we propose the supervised twin-bottleneck hashing, where a classifier is applied on top of the binary



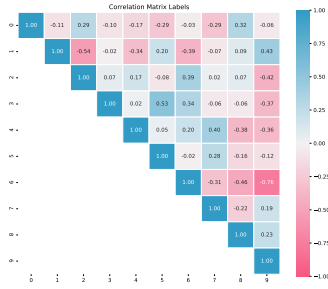
(a) CIFAR-10, TBH



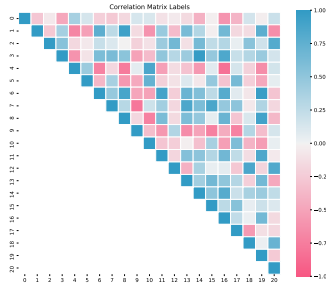
(b) NUS-WIDE, TBH



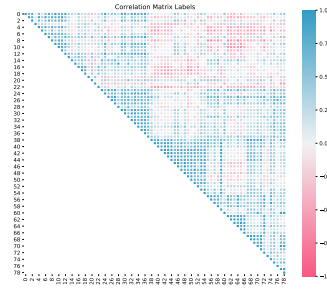
(c) MS-COCO, TBH



(d) CIFAR-10, STBH, $\eta = 100, \gamma = 20$



(e) NUS-WIDE, STBH, $\eta = 20, \gamma = 10$



(f) MS-COCO, STBH, $\eta = 30, \gamma = 30$

Figure 7. Correlation matrix of labels for the TBH model (upper) and STBH model (lower) with chosen η, γ values.

bottleneck of the original TBH model [26]. The supervised learning enables the network to incorporate class labels, which provide complementary information independent of feature vectors, help separate data points with different labels, and mitigate strong correlations of classes. Experiments conducted on three representative datasets show a statistically significant improvement against the original TBH model at a small modification cost. Furthermore, STBH is compared to other supervised methods of deep hashing, which reveals our results are competitive to the state-of-art results.

In addition, we briefly discuss the class imbalance problem that is hardly considered in previous hashing papers and also mention some existing possible solutions. More works can be performed to quantify the performance effect due to the imbalance, and deal with this problem in the future.

A. P-value computation in Hypothesis Testing

In the paper, we want to examine whether the STBH model performs better than the TBH model. More specifically, we would like to check if the mean of results from STBH (μ_2) is greater than that from TBH (μ_1). For this, we adopt the hypothesis testing with the following two hy-

potheses:

$$\begin{aligned} H_0 &: \mu_2 \leq \mu_1 \\ H_1 &: \mu_2 > \mu_1 \end{aligned} \tag{A.1}$$

where H_0 is the null hypothesis, H_1 is the alternative hypothesis, μ_1 is the population mean of results from the TBH model, and μ_2 is the population mean of the STBH model.

This is a question on the test of the difference between two population means. The distribution is assumed to be Gaussian. Considering the number of the samples is small (6 in our paper), we adopt the t-distribution $f_\nu(t)$ for the test statistic with ν the degree of freedom. And the test statistic t^* is computed as follows:

$$t^* = \frac{(\bar{X}_1 - \bar{X}_2)}{\left(\frac{s_1^2}{n_1} + \frac{s_2^2}{n_2}\right)^{1/2}} \tag{A.2}$$

where \bar{X}_1 (\bar{X}_2) is the samples' mean of TBH (STBH), s_1 (s_2) is the samples' standard deviation of TBH (STBH), and n_1 (n_2) is the number of samples, which is 6 in our case. In addition, the degree of freedom of the t-distribution is given

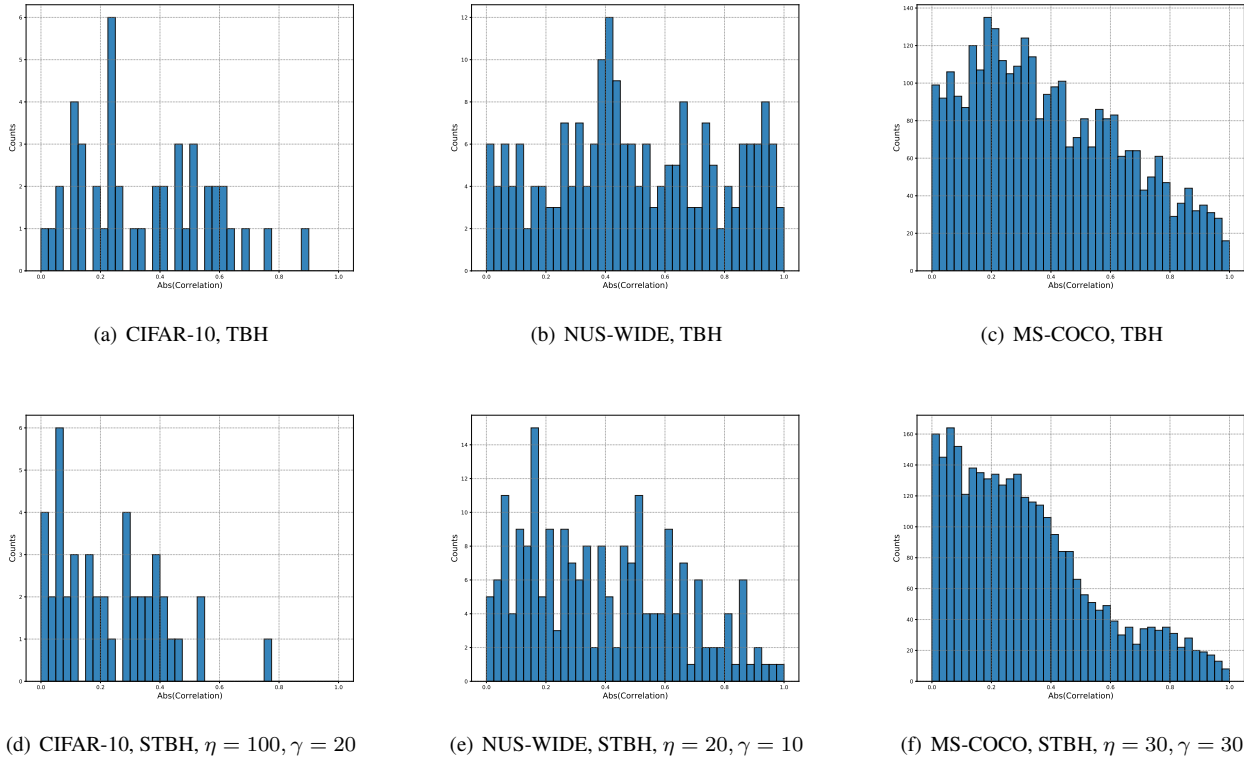


Figure 8. Histograms of absolute values of correlations for the TBH model (upper) and STBH model (lower) with chosen η, γ values.

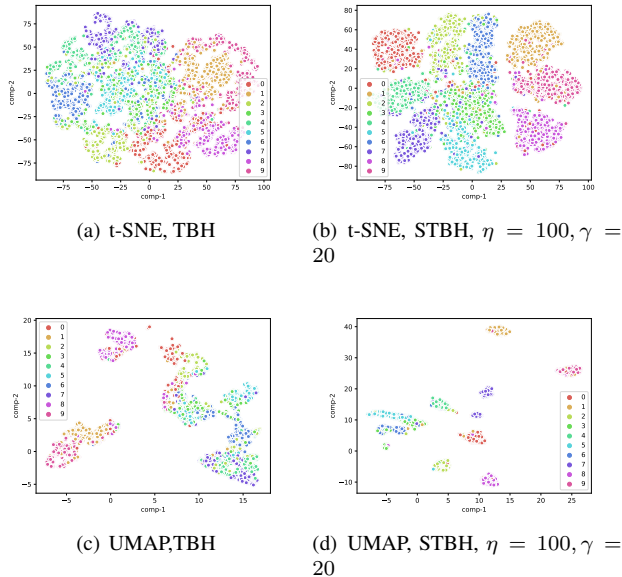


Figure 9. Visualization plots of CIFAR-10 from encoded binary codes with t-SNE (upper) and UMAP (lower) techniques for the TBH model (left) and STBH model (right).

by:

$$\nu = \frac{\left(\frac{s_1^2}{n_1} + \frac{s_2^2}{n_2}\right)^2}{\frac{(s_1^2/n_1)^2}{n_1} + \frac{(s_2^2/n_2)^2}{n_2}} \quad (\text{A.3})$$

We can then compute p-value from the t-distribution with the computed test statistic as:

$$p = \int_{t^*}^{\infty} f_{\nu}(t) dt \quad (\text{A.4})$$

The smaller the p-value is, the more evidence we have to reject the H_0 and accept the H_1 hypothesis.

References

- [1] Martín Abadi, Paul Barham, Jianmin Chen, Zhifeng Chen, Andy Davis, Jeffrey Dean, Matthieu Devin, Sanjay Ghemawat, Geoffrey Irving, Michael Isard, et al. Tensorflow: A system for large-scale machine learning. In *12th {USENIX} symposium on operating systems design and implementation ({OSDI} 16)*, pages 265–283, 2016. 4
- [2] Fatih Cakir, Kun He, and Stan Sclaroff. Hashing with binary matrix pursuit. In *Proceedings of the European conference on computer vision (ECCV)*, pages 332–348, 2018. 1, 8
- [3] Francisco Charte, Antonio J Rivera, María J del Jesus, and Francisco Herrera. Mlsmote: Approaching imbalanced multilabel learning through synthetic instance generation. *Knowledge-Based Systems*, 89:385–397, 2015. 5
- [4] Francisco Charte, Antonio J Rivera, and J María. del Jesus, and Francisco Herrera. 2015. “addressing imbalance in multilabel classification: Measures and random resampling algorithms.”. *Neurocomputing*. <https://doi.org/10.1016/j.neucom.2014.05.011>. 5

- [5] Nitesh V Chawla, Kevin W Bowyer, Lawrence O Hall, and W Philip Kegelmeyer. Smote: synthetic minority over-sampling technique. *Journal of artificial intelligence research*, 16:321–357, 2002. [5](#)
- [6] Ken Chen, Bao-Liang Lu, and James T Kwok. Efficient classification of multi-label and imbalanced data using min-max modular classifiers. In *The 2006 IEEE International Joint Conference on Neural Network Proceedings*, pages 1770–1775. IEEE, 2006. [5](#)
- [7] Tat-Seng Chua, Jinhui Tang, Richang Hong, Haojie Li, Zhiping Luo, and Yantao Zheng. Nus-wide: a real-world web image database from national university of singapore. In *Proceedings of the ACM international conference on image and video retrieval*, pages 1–9, 2009. [4](#)
- [8] Thanh-Toan Do, Anh-Dzung Doan, and Ngai-Man Cheung. Learning to hash with binary deep neural network. In *European Conference on Computer Vision*, pages 219–234. Springer, 2016. [1](#)
- [9] Alberto Fernández, Salvador Garcia, Francisco Herrera, and Nitesh V Chawla. Smote for learning from imbalanced data: progress and challenges, marking the 15-year anniversary. *Journal of artificial intelligence research*, 61:863–905, 2018. [5](#)
- [10] Andrés Felipe Giraldo-Forero, Jorge Alberto Jaramillo-Garzón, José Francisco Ruiz-Muñoz, and César Germán Castellanos-Domínguez. Managing imbalanced data sets in multi-label problems: a case study with the smote algorithm. In *Iberoamerican Congress on Pattern Recognition*, pages 334–342. Springer, 2013. [5](#)
- [11] Yunchao Gong, Svetlana Lazebnik, Albert Gordo, and Florent Perronnin. Iterative quantization: A procrustean approach to learning binary codes for large-scale image retrieval. *IEEE transactions on pattern analysis and machine intelligence*, 35(12):2916–2929, 2012. [1](#)
- [12] Jianjun He, Hong Gu, and Wenqi Liu. Imbalanced multi-modal multi-label learning for subcellular localization prediction of human proteins with both single and multiple sites. *PloS one*, 7(6):e37155, 2012. [5](#)
- [13] Yosuke Igarashi and Kazuhiro Fukui. 3d object recognition based on canonical angles between shape subspaces. In *Asian Conference on Computer Vision*, pages 580–591. Springer, 2010. [5](#)
- [14] Herve Jegou, Matthijs Douze, and Cordelia Schmid. Product quantization for nearest neighbor search. *IEEE transactions on pattern analysis and machine intelligence*, 33(1):117–128, 2010. [1](#)
- [15] Thomas N Kipf and Max Welling. Semi-supervised classification with graph convolutional networks. *arXiv preprint arXiv:1609.02907*, 2016. [1](#), [2](#)
- [16] Bartosz Krawczyk. Learning from imbalanced data: open challenges and future directions. *Progress in Artificial Intelligence*, 5(4):221–232, 2016. [5](#)
- [17] Alex Krizhevsky, Geoffrey Hinton, et al. Learning multiple layers of features from tiny images. 2009. [4](#)
- [18] Cunhe Li and Guoqiang Shi. Improvement of learning algorithm for the multi-instance multi-label rbf neural networks trained with imbalanced samples. *J. Inf. Sci. Eng.*, 29(4):765–776, 2013. [5](#)
- [19] Qi Li, Zhenan Sun, Ran He, and Tieniu Tan. Deep supervised discrete hashing. *arXiv preprint arXiv:1705.10999*, 2017. [1](#), [8](#)
- [20] Wu-Jun Li, Sheng Wang, and Wang-Cheng Kang. Feature learning based deep supervised hashing with pairwise labels. *arXiv preprint arXiv:1511.03855*, 2015. [1](#), [8](#)
- [21] Tsung-Yi Lin, Michael Maire, Serge Belongie, James Hays, Pietro Perona, Deva Ramanan, Piotr Dollár, and C Lawrence Zitnick. Microsoft coco: Common objects in context. In *European conference on computer vision*, pages 740–755. Springer, 2014. [4](#)
- [22] Haomiao Liu, Ruiping Wang, Shiguang Shan, and Xilin Chen. Deep supervised hashing for fast image retrieval. In *Proceedings of the IEEE conference on computer vision and pattern recognition*, pages 2064–2072, 2016. [1](#)
- [23] Wei Liu, Jun Wang, Rongrong Ji, Yu-Gang Jiang, and Shih-Fu Chang. Supervised hashing with kernels. In *2012 IEEE Conference on Computer Vision and Pattern Recognition*, pages 2074–2081. IEEE, 2012. [1](#)
- [24] Leland McInnes, John Healy, and James Melville. Umap: Uniform manifold approximation and projection for dimension reduction. *arXiv preprint arXiv:1802.03426*, 2018. [7](#)
- [25] Yuxin Peng, Jian Zhang, and Zhaoda Ye. Deep reinforcement learning for image hashing. *IEEE Transactions on Multimedia*, 22(8):2061–2073, 2019. [1](#), [8](#)
- [26] Yuming Shen, Jie Qin, Jiaxin Chen, Mengyang Yu, Li Liu, Fan Zhu, Fumin Shen, and Ling Shao. Auto-encoding twin-bottleneck hashing. In *Proceedings of the IEEE/CVF Conference on Computer Vision and Pattern Recognition*, pages 2818–2827, 2020. [1](#), [2](#), [4](#), [9](#)
- [27] Le Song. Stochastic generative hashing. In *ICML*, 2017. [2](#)
- [28] Christian Szegedy, Vincent Vanhoucke, Sergey Ioffe, Jonathon Shlens, and Zbigniew Wojna. Rethinking the inception architecture for computer vision. *CoRR*, abs/1512.00567, 2015. [4](#)
- [29] Muhammad Atif Tahir, Josef Kittler, and Ahmed Bouridane. Multilabel classification using heterogeneous ensemble of multi-label classifiers. *Pattern Recognition Letters*, 33(5):513–523, 2012. [5](#)
- [30] Muhammad Atif Tahir, Josef Kittler, and Fei Yan. Inverse random under sampling for class imbalance problem and its application to multi-label classification. *Pattern Recognition*, 45(10):3738–3750, 2012. [5](#)
- [31] Gorn Tepvorachai and Chris Papachristou. Multi-label imbalanced data enrichment process in neural net classifier training. In *2008 IEEE International Joint Conference on Neural Networks (IEEE World Congress on Computational Intelligence)*, pages 1301–1307. IEEE, 2008. [5](#)
- [32] Ilya Tolstikhin, Olivier Bousquet, Sylvain Gelly, and Bernhard Schölkopf. Wasserstein auto-encoders. *arXiv preprint arXiv: 1711.01558*, 2017. [2](#), [3](#)
- [33] Laurens Van der Maaten and Geoffrey Hinton. Visualizing data using t-sne. *Journal of machine learning research*, 9(11), 2008. [7](#)
- [34] Jun Wang, Wei Liu, Andy X Sun, and Yu-Gang Jiang. Learning hash codes with listwise supervision. In *Proceedings of the IEEE International Conference on Computer Vision*, pages 3032–3039, 2013. [1](#)

- [35] Jingdong Wang, Ting Zhang, Nicu Sebe, Heng Tao Shen, et al. A survey on learning to hash. *IEEE transactions on pattern analysis and machine intelligence*, 40(4):769–790, 2017. [1](#)
- [36] Xiaofang Wang, Yi Shi, and Kris M Kitani. Deep supervised hashing with triplet labels. In *Asian conference on computer vision*, pages 70–84. Springer, 2016. [1](#), [8](#)
- [37] Zhenzhen Wang, Weixiang Hong, and Junsong Yuan. Deep reinforcement learning with label embedding reward for supervised image hashing. *arXiv preprint arXiv:2008.03973*, 2020. [1](#), [8](#)
- [38] Yair Weiss, Antonio Torralba, Robert Fergus, et al. Spectral hashing. In *Nips*, volume 1, page 4. Citeseer, 2008. [1](#)
- [39] Rongkai Xia, Yan Pan, Hanjiang Lai, Cong Liu, and Shuicheng Yan. Supervised hashing for image retrieval via image representation learning. In *Proceedings of the AAAI conference on artificial intelligence*, volume 28, 2014. [4](#)
- [40] Xin Yuan, Liangliang Ren, Jiwen Lu, and Jie Zhou. Relaxation-free deep hashing via policy gradient. In *Proceedings of the European Conference on Computer Vision (ECCV)*, pages 134–150, 2018. [1](#), [8](#)
- [41] Ting Zhang, Chao Du, and Jingdong Wang. Composite quantization for approximate nearest neighbor search. In *International Conference on Machine Learning*, pages 838–846. PMLR, 2014. [1](#)
- [42] Han Zhu, Mingsheng Long, Jianmin Wang, and Yue Cao. Deep hashing network for efficient similarity retrieval. In *Proceedings of the AAAI Conference on Artificial Intelligence*, volume 30, 2016. [1](#)